ELM Transport in the JET Scrape-Off Layer

R.A. Pitts 1), P. Andrew 2), G. Arnoux 3), T. Eich 4), W. Fundamenski 2), E. Gauthier 3), A. Huber 5), S. Jachmich 6), C. Silva 7), D. Tskhakaya 8)* and JET EFDA Contributors[1]

1) École Polytechnique Fédérale de Lausanne (EPFL), Centre de Recherches en Physique des Plasmas, Association Euratom – Confédération Suisse, 1015 Lausanne, Switzerland
2) EURATOM-UKAEA Fusion Association, Culham Science Centre, Abingdon, Oxon OX14 3DB, UK
3) Association EURATOM-CEA, DSM-DRFC, CEA Cadarache, 13108 Saint Paul lez Durance, France
4) Max-Planck-Institut für Plasmaphysik, IPP-EURATOM Association, D-85748 Garching, Germany
5) Institut für Plasmaphysik, FZJ, EURATOM Association, TEC, D-52425 Jülich, Germany
6) Laboratory for Plasmaphysics, Ecole Royale Militaire/Koninklijke Militaire School, EURATOM-Association "Belgian State", Brussels, Belgium, Partners in the TEC
7) Associação Euratom/IST, Centro de Fusão Nuclear, Instituto Superior Técnico, 1049-001 Lisboa, Portugal
8) Univ. Innsbruck, Institute for Theoretical Physics, Association EURATOM-ÖAW, A-6020 Innsbruck, Austria
*Permanent address: Institute of Physics Georgian Academy of Sciences, 380077 Tbilisi, Georgia
Email contact of main author: richard.pitts@epfl.ch

Abstract: This contribution summarises a number of aspects of the experimental and modelling programme at JET aimed at improving the characterisation and understanding of ELM transport in the scrape-off layer (SOL). Divertor target energy deposition asymmetries favouring the inner target for the ion $\mathbf{B}\times\nabla B$ drift directed towards the X-point are observed with infra-red (IR) thermography. Particle-in-Cell kinetic calculations of the parallel ELM heat transport have been made for a range of ELM energies, showing the detailed time response of target sheath heat transmission factors and indicating that electrons deposit ~30% of the ELM energy. A transient model of ELM filament energy evolution has been developed at JET and is able to reproduce a number of experimental observations, including the high ion energies observed in the far SOL using an electrostatic retarding field electrostatic analyser (RFA) and estimates of ELM heat fluxes deposited on main chamber limiters. During the ELM, the RFA and a second, SOL turbulence probe, clearly show the presence of coherent spikes on the hot ion flux, the plasma flux and the electron temperature. Filamentary structures have also been seen for the first time on JET in the power deposition on main wall limiters and upper dump plate surfaces using a new wide angle IR camera system. The probe signals are interpreted as the arrival of interspaced, toroidally rotating plasma filaments, with successive filaments carrying less energy. They are also consistent with the ELM disturbance entering the SOL on the outboard side and launching a sound wave disturbance along field lines.

1. Introduction

Edge Localised Modes (ELMs) are universally recognised as one of the greatest threats to the viability of ITER and future tokamak power plants. In ITER, extrapolations from JET predict that Type I ELMs in the Q_{DT} = 10 baseline scenario will expel between 3-8% of the 350 MJ plasma stored energy, depositing energy fluxes of 0.6 – 3.4 MJm^{-2} on the divertor targets [1]. Concerns are now being raised that even the low end of this range may be too high from the point of view of target lifetime [2]. Observations are also showing that ELM power fluxes can extend to main chamber walls, constituting a potential threat to main wall erosion in long pulse, higher power devices [3]. By compiling a number of recent observations from JET supported by new theoretical analysis, this paper aims to show how our understanding of both the parallel and perpendicular ELM transport in the SOL is evolving.

2. Parallel transport and ELM-target interactions

2.1 In-out energy asymmetries

In addition to the critical question of the absolute ELM power load experienced on the divertor targets, the power sharing between the inner and outer targets is also an important parameter. Tokamak

[1]See the Appendix of M. L.Watkins et al., Fusion Energy 2006 (Proc. 21st Int. Conf. Chengdu, 2006) IAEA, (2006)

operation with normal, or forward (FWD-B) toroidal field direction (i.e. with the ion **B**×∇B drift direction downwards) is known to lead to higher power deposition on the outboard target during inter-ELM periods. This is a result of the combined effects of toroidal geometry, Shrafanov shift, the tendency for increased perpendicular energy transport to the outboard SOL and classical drift related energy fluxes, which drive power preferentially to the outboard target for FWD-B. Toroidal field reversal experiments on JET have demonstrated these effects rather clearly [4,5], finding ELM averaged target energy deposition asymmetries (using target tile calorimetry) of E_o/E_i ~3 at the highest SOL powers, P_{SOL}, during FWD-B H-modes, compared with an offset of E_o/E_i ~ 2 at low power in L-mode. These trends are consistent with a field dependent component which scales approximately with P_{SOL}, or more correctly, power/per particle into the SOL, as would be expected from poloidal drift contributions [4].

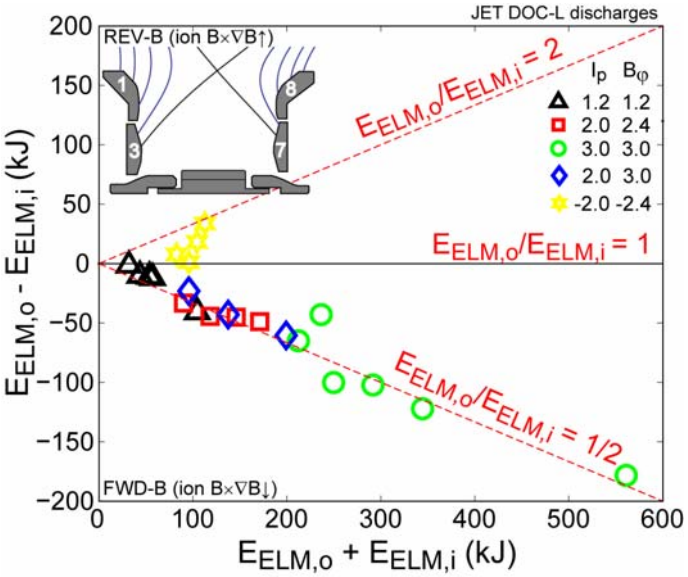

Fig. 1: *Demonstrating the observed Type I ELM energy deposition asymmetry in favour of the inner target for FWD-B in the JET MarkIISRP gas box divertor. I_p and B_φ in MA and T respectively.*

The observation during this "global" analysis (i.e. target energy balance integrated over the entire discharge) of a lower E_o/E_i ratio for given P_{SOL} in L-mode compared with Type I ELMing H-mode in both FWD-B and REV-B discharges, already indicated a possible asymmetry in the ELM energy deposition favouring the inner target. This has now been further quantified by a detailed study of the ELM energy deposition itself using infra-red (IR) thermography. Such analysis is challenging, requiring that the presence of co-deposited surface layers be properly accounted for. These layers are particularly problematic at the inner target, always a region of net deposition on JET for FWD-B operation, but essentially absent in the outer strike point vicinity, a zone of net erosion or zero net-redeposition [6,7]. They have the effect of yielding an artificially high surface temperature rise during transient events. Careful analysis, using inverse solutions to the heat conduction equation coupled with tile calorimetry to calibrate total energy balance, allows the transient power flux to be correctly deconvoluted from the temperature rise [8]. The result of this exercise for a range of discharges with varying ELM pedestal energy loss in the range W_{ELM} = 0.05 → 1.0 MJ is shown in Fig. 1, mostly for the case of FWD-B, but with the few available points from the 2003 REV-B campaign also included. All data correspond to experiments performed in the MarkIISRP gas box divertor using the so-called Diagnostic Optimised Configuration, where "DOC-L" denotes a variant of this equilibrium with strike points located on the lower vertical tiles of the divertor (see inset in Fig. 1).

In FWD-B, over a range of ELM target energy loads (both inner and outer) from 100 → 500 kJ, the out/in target energy ratio closely satisfies $E_{ELM,o}/E_{ELM,i}$ = 0.5 and has no dependence on pedestal collisionality. At lower values of energy, below ~100 kJ, there is more scatter in the data, to a large extent due to the effect of surface layers and lower IR signals, which make interpretation harder at lower energies on JET. In REV-B experiments, where the range of ELM energies was restricted to low values, there is a clear trend for a reversal of the target asymmetry, though the scatter in this restricted dataset prevents the derivation of a clear scaling. It is significant, however, that $E_{ELM,o}/E_{ELM,i}$ ~ 2 has been found for REV-B on AUG in the low energy range ($E_{ELM,o}$+$E_{ELM,i}$ < 20 kJ) for a much larger dataset [9]. There, IR measurements are adapted to the lower ELM energies and the spread seen in $E_{ELM,o}/E_{ELM,i}$ cannot be attributed to experimental error. In FWD-B, $E_{ELM,o}/E_{ELM,i} \leq 2$ on AUG (also for $E_{ELM,o}$+$E_{ELM,i}$ < 20 kJ) similar to the JET findings, demonstrating that this is a real target ELM energy asymmetry. More importantly, it is in the opposite direction to the observed (and understood) inter-ELM asymmetry and therefore acts to reduce the total (i.e. ELM-averaged) ratio of E_o/E_i. Although the explanation for the observed in-out asymmetry has yet to be found, a strong, field direction dependent correlation has been found between the direction and magnitude of charge flowing

through the target plates and the energy difference, $E_{ELM,o}$-$E_{ELM,i}$ [9]. This behaviour cannot be explained by thermoelectric current flows and seems instead to be drift related, possibly due to diamagnetic current loss during the ELM. In the absence of net current, $E_{ELM,o}/E_{ELM,i} = 1$ is observed in these AUG measurements. This is what would be expected on the basis of a recent model developed at JET of parallel ELM filament energy losses [10] which has had considerable success in matching a number of alternative observations of ELM dynamics (see Section 3.2). In the kinetic form of this 1D model, the description of the transient predicts a ratio of peak heat fluxes inversely proportional to the ratio of midplane to target connection lengths ($L_{||o}/L_{||i} \sim 2$ on JET) and $E_{ELM,o}/E_{ELM,i} = 1$ by definition since currents are neglected.

Recent evidence from new measurements with the upgraded bolometer diagnostic on JET [11] support similar observations on AUG [12] that radiation in the divertor during the ELM is strongly weighted to the inner divertor volume, with the ratio $P_{RAD,i}/P_{RAD,o}$ increasing by as much as a factor 2 compared with inter-ELM values (where typically $P_{RAD,i}/P_{RAD,o} \sim 2$ on JET). This is also consistent with higher energies being deposited on the inner than at the outer target during the ELM, though the differing pre-ELM plasma (more dense and colder at the inner) and the presence of co-deposited layers complicate the interpretation and more data across a wider range of ELM energies is required to quantify the total energy balance.

2.2 Particle-in-cell (PIC) kinetic modelling

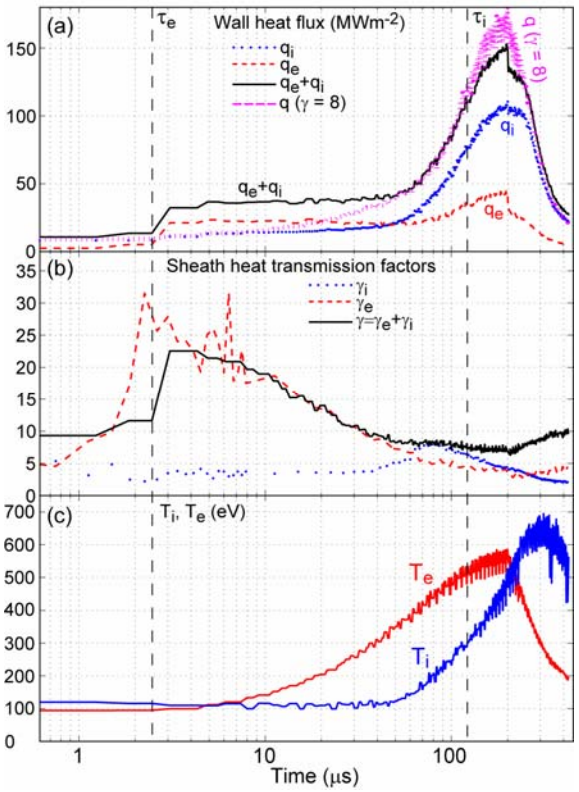

Fig. 2: *Time dependence of simulated (a) $q_{e,i}$ (b) sheath transmission factors and (c) $T_{e,i}$ for a 120 kJ ELM. Parameters τ_i, τ_e are the ion and electron timescales for propagation down the SOL from the upstream pedestal. Also shown in (a) is the target power obtained if constant $\gamma = 8$ is assumed*

For anything but the smallest ELMs, the parallel propagation of heat from the point of release to the divertor targets is inherently a kinetic situation. Edge fluid-Monte Carlo codes, which provide realistic descriptions of the steady-state SOL plasma in 2D, cannot adequately describe this kinetic transport and in particular must employ limiting coefficients for parallel SOL heat fluxes (not discussed here) and those at the sheath edge boundary, which represents the limit of validity of the fluid simulation.

These coefficients ultimately determine the target heat fluxes predicted by the code and are usually assumed spatially and temporally constant during the transient. That this is clearly not the case has been known for some time from 1d3v PIC simulations, which have been steadily increasing in complexity in recent years [13-15]. One such code, BIT1, is being applied to ELM modelling of the JET SOL. The code includes particle collisions, inclined magnetic fields at the targets (~5º), and significantly increased resolution compared to earlier simulations reported in [14] for JET (~6000 poloidal grid cells, giving very low shortening factors). Secondary electron emission (s.e.e.) at the targets has been neglected since, unlike the findings in [13], its inclusion is not observed to significantly affect the target electron power load in these JET runs. The ELM is simulated by introducing an ambipolar source of particles, S, specified using a density n_{ped} with a cosine spatial distribution of given extent centred on the midpoint between two targets. The total ELM energy is then given by $W_{ELM} = 3S(T_{i,ped}+T_{e,ped})Vt_{ELM}/2$ with t_{ELM} the ELM duration, usually fixed at 200 μs (a typical ELM duration on JET), and $V = L_{pol}2\pi RdR$ the SOL "volume" into which the ELM energy is assumed to deposit (L_{pol} is the poloidal extent of the region, determined by an assumed connection length of $L_{||} = 40$ m, dR ~ 0.1 m is the "radial extent" of the 1D

SOL). Assuming $T_{i,ped} = T_{e,ped} = T_{ped}$, a number of these extremely CPU intensive simulations have been performed covering an approximate range of n_{ped}, T_{ped} found on JET, giving $W_{ELM} = 0.025 \rightarrow 2.5$ MJ, where the latter is currently beyond JET's capabilities, but would represent a rather small Type I ELM on ITER. Figure 2 illustrates the time dependence during the ELM of the target heat fluxes, q_a, the sheath heat transmission factors [16], $\gamma_a = q_a/\Gamma_a T_a$ (a = i,e for ions or electrons, Γ_a the particle fluxes) evaluated at the sheath edge and the local temperatures, T_a for a case with T_{ped} = 1.5 keV, $n_{ped} = 1.5 \times 10^{19}$ m^{-3}, W_{ELM} = 122 kJ. Table 1 compiles the full database of simulations, in terms of the key important parameters concerning target heat loads.

W_{ELM} (MJ)	n_{ped} (10^{19}m^{-3})	T_{ped} (keV)	ν^*_{ped}	t_{ELM} (μs)	Q_e (MJm^{-2})	Q_i (MJm^{-2})	Q_e/Q_i	q_w^{max} (GWm^{-2})	γ_e^{max}	γ_i^{max}
0.024	1.5	0.5	2.0	200	0.0021	0.006	0.35	0.032	7.5	4.4
0.078	5	0.5	6.7	200	0.0053	0.017	0.31	0.105	13.5	5.8
0.11	5	1.5	0.74	53	0.0078	0.027	0.29	0.317	65	11.2
0.122	1.5	1.5	0.22	200	0.0087	0.023	0.38	0.153	31.5	8.4
0.40	5	1.5	0.74	200	0.024	0.082	0.29	0.539	65	11.2
0.74	1.5	5.0	0.02	200	0.0653	0.125	0.52	0.962	98	19.7
0.80	5	1.5	0.74	400	0.0457	0.14	0.32	0.575	65	11.2
1.22	15	1.5	2.22	200	0.067	0.235	0.29	1.420	186	16.3
2.46	5	5.0	0.07	200	0.195	0.475	0.41	3.255	580	42

Tab. 1: *Key parameters for target loading and ELM dynamics from database of BIT1 PIC simulations of the JET SOL. Q_i, Q_e are target energies integrated over t_{ELM}+150μs, ν^*_{ped} is the pedestal collisionality and q_w^{max}, γ_e^{max}, γ_i^{max} are maximum values during the ELM*

Figure 2a demonstrates clearly the abrupt rise of q_e on the electron transit timescale, $\tau_e \sim L_{\|}/v_{Tped,}$ followed by the main ELM front propagating on the ion sonic timescale, $\tau_i \sim L_{\|}/c_{s,ped}$, ($c_{s,ped}$ is the ion sound speed evaluated at T_{ped}), bringing the bulk of the ELM energy to the target. Local temperatures (Fig. 2c) rise throughout the ELM pulse, reaching ~40% of T_{ped}. The heat transmission factors (Fig. 2b) begin at their classically expected Maxwellian values, $\gamma_e \sim 5$, $\gamma_i = 2 \rightarrow 3.5$, with γ_e rising by a factor ~6 on the timescale τ_e, as pedestal electrons arriving at the target drive the formation of a high sheath potential (~2-3 T_{ped}). As shown in Table 1, this enhancement in γ_e can be up to two orders of magnitude for the largest ELMs simulated. Thermal ions are drawn from the sheath region by the increased potential, increasing q_i slightly at the electron pulse arrival. Thereafter, the situation stabilises until the arrival of the bulk ion pulse on timescale τ_i, provoking an approximate factor 2 increase in γ_i over the asymptotic pre-ELM Maxwellian value and providing the peak in the ELM target heat flux. The sharp drop in q_e at 200 μs signals the end of the ELM heat pulse injected upstream. The "classical" estimate of q_w, with a constant $\gamma = \gamma_e + \gamma_i = 8$ assumed by the fluid codes is also included in Fig. 2a, demonstrating that although the electron contribution to the target heat load in the first ~50 μs of the ELM would be underestimated, the total integrated energy (dominated by the ions) would be relatively well reproduced. Note that the "total" γ in Fig. is computed by normalising γ_i to the electron flux and temperature: $\gamma = \gamma_e + \gamma_i \Gamma_i T_i / \Gamma_e T_e$. For given values of W_{ELM}, the simulated peak target heat fluxes, q_w^{max}, are a factor 2-3 lower than IR measured values, a large proportion of which can be accounted for by the poor IR camera time resolution.

The ratio Q_e/Q_i in Table 1 is approximately independent of W_{ELM} and hence of any particular T_{ped}, n_{ped} combination. Its average value across the simulation database is $Q_e/Q_i = 0.35$, with the electrons conveying at most ~50% of the ELM electron energy to the target. The highest factors occur at high T_{ped}, when collisional coupling to the ions decreases.

3. Perpendicular transport and ELM wall interactions

3.1 Filamentary structure

The picture of an ELM in the SOL as a structure propagating radially as a series of rotating, field aligned filaments is being increasingly confirmed by observations in various tokamaks [17,18]. An early indication that these filaments can interact with the main chamber walls in JET was obtained by subtracting two visible images of main chamber recycling, thus revealing contact with outboard limiters and upper baffle, as well as a faint, but visible helical stripe [19]. This has very recently been

confirmed by first measurements with a new, wide angle IR camera system based on ITER relevant reflective optics which views the main chamber and divertor [20,21]. Figure 3 compiles images of two separate Type I ELM events (W_{ELM} ~ 150 kJ) seen with the new camera in two different plasma configurations, each with different points of closest contact to first limiting surfaces beyond the separatrix. These IR images are the difference between successive frames (10 ms separation) captured during 300 μs snapshots before and during the ELM. The slow, full frame time resolution (10 ms) of the camera means that few such events are found in any particular discharge. When the plasma is close to the outer limiters, discrete, helically aligned zones of excess power deposition are found on successive limiters. These are found in different poloidal locations for each ELM and are similar to the IR main chamber observations reported from AUG [22]. For an equilibrium where flux surfaces beyond the separatrix first intersect the upper dump plates, multiple filaments are observed, though the proximity to an upper X-point means that the field aligned nature is harder to discern. Again, similar findings have first been reported from observations at the AUG divertor targets [18]. In no case is any interaction found on high field side main chamber structures, likely a result of the large high field side separatrix-wall gaps.

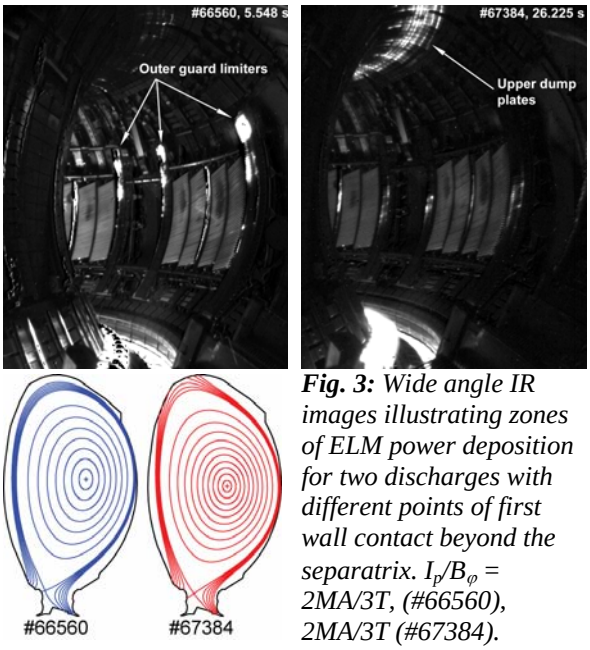

Fig. 3: *Wide angle IR images illustrating zones of ELM power deposition for two discharges with different points of first wall contact beyond the separatrix. I_p/B_φ = 2MA/3T, (#66560), 2MA/3T (#67384).*

This filamentary structure in the far SOL is also picked up by fast reciprocating probes which enter the vacuum vessel at the top low field side of the poloidal cross-section. Two such probes have recently been used on JET to study ELMs, a retarding field analyser (RFA) for measurements of the SOL T_i [23] and a probe dedicated to turbulent transport studies (TTP), capable also of following the local T_e and effective $\mathbf{E_\theta \times B}$ driven radial velocity on a fast timescale [24]. The time traces from the TTP for a single event (W_{ELM} ~100 kJ) captured in the far SOL close to the outer guard limiter radius (separatrix-wall gap, Δ_{SOL} ~40 mm, mapped to the outer midplane). Evidently, the ELM event is composed of a number of discrete filaments, with T_e in each filament rising to at most a few times the pre-ELM value and perpendicular propagation velocities reaching v_r ~ 1 kms^{-1}. A similar picture is obtained with the RFA probe, an example of which is shown in Fig. 5, also for Δ_{SOL} ~ 40 mm, but with W_{ELM} ~ 50 kJ in a hydrogen plasma. The probe is bi-directional, with sensors facing into both the outer and inner divertors along field lines. The ratio of parallel ion fluxes to the RFA entrance slit plates clearly favours the ion drift direction, namely from outer to inner divertor along the total magnetic field. Using the Mach probe capability of the TTP leads to the same conclusion. Given the probe location, the obvious conclusion is that the ELM is a phenomenon which tends to be released on the low field side, launching a sound wave disturbance along field lines (see schematic in Fig. 5e). It is worth noting that the ELMs in Figs. 4,5 are relatively low energy events (for JET), obtained in plasmas with high pedestal collisionalities (ν^*_{ped} ~ 0.5), since the use of these rather delicate probes during more energetic events, even in the far SOL, is problematic.

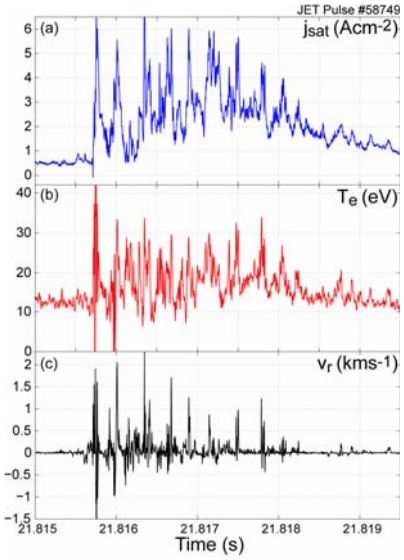

Fig. 4: *Results from the TTP probe [24] for a single ELM in a plasma with I_p/B_φ = 2MA/2.45T illustrating the filamentary structure of the parallel ion flux (a), T_e (b) and effective radial velocity (c).*

The collector currents registered by the RFA (Fig. 5d) correspond to particles which have been able to overcome the internal +400V fixed bias potentials and thus to ions with at least this energy [23]. Successive filaments within the ELM produce lower collector currents, implying that

each carries ions with lower energies. There is a similar trend in the T_e excursions seen in the TTP signals (Fig. 4b). The picture then of the ELM is of a series of interspaced, toroidally rotating filaments, sweeping past the probe on a timescale of order 2 ms, approximately a factor 10 longer than the ELM duration as seen on magnetic signals. Since each successive filament must travel further to reach the probe, parallel energy losses are higher and measured filament temperatures are lower. It is also very clear from the high time resolution TTP data that each filament in the ELM itself possesses a sub-structure, consistent with the break-up of the individual filaments as they propagate radially. Qualitatively, this behaviour is what would be expected if radial interchange motions governed the perpendicular motion [25].

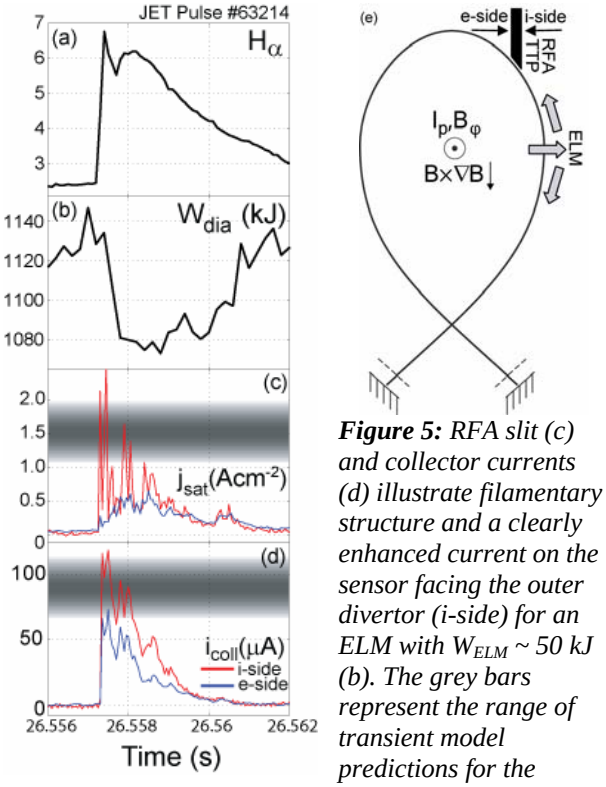

Figure 5: *RFA slit (c) and collector currents (d) illustrate filamentary structure and a clearly enhanced current on the sensor facing the outer divertor (i-side) for an ELM with W_{ELM} ~ 50 kJ (b). The grey bars represent the range of transient model predictions for the plasma and hot ion flux.*

3.2 Modelling the transient

A new model of transient parallel energy losses in the SOL has been developed at JET and has had a number of notable successes in matching the ELM observations described here [10]. The model contains both a kinetic and fluid treatment, with analytic functions derived from the kinetic approach having had considerable success in matching the time evolution and magnitude of γ_e,γ_i predicted by the PIC simulations shown in Fig. 2. It is, however, the fluid approach that has been most applied thus far in comparison with experiment.

A number of questions still remain unanswered regarding the evolution of the ELM instability in the pedestal region, particularly with regard to precisely when and where, during the ELM event, filaments separate and begin to propagate independently in the SOL. At some point, however, they must begin to lose their particle, energy and current content to the divertor targets. In the model, t = 0 is defined as the time at which such parallel losses begin. In the absence of reconnection, this occurs when the filament reaches the separatrix location, whilst if reconnection is present from the outset, t = 0 corresponds to the pedestal location. More generally, parallel losses can be assumed to begin at some mid-pedestal position. A simplified description of the ELM filament is obtained by solving the conservation equations of mass and energy together with parallel losses in the filament frame of reference. Time and radius are related by the filament radial velocity, which is prescribed in the model. Density is removed roughly at the plasma sound speed, $\tau_n = L_{||}/c_s$, while energy is removed by a combination of convection and conduction. In a second stage of the model, a further reduction in the filament quantities due to radial broadening is estimated by assuming semi-adiabatic ($T \propto n^{\gamma-1} \propto n^{1/3}$) expansion [10].

The shaded regions in Fig. 6 represent the range of the transient model prediction of the RFA collector and slit plate ion-side currents using an analytic description of RFA function [23] and assuming $v_r = 0.6$ kms^{-1} (extrapolated from an earlier detailed study of ELM-limiter interactions [26]), semi-adiabatic radial broadening and a range of filament starting points from pedestal top to separatrix. Values of T_i, T_e and n_e in the range 100 → 150 eV, 40 → 75 eV and 0.75 → 1.0x10^{19} m^{-3} respectively are predicted at the probe location, demonstrating that T_i falls less rapidly than T_e as the filament crosses the SOL (as expected given the much faster rates of electron heat loss) and that ions arriving at limiter surfaces can do so with a significant fraction of $T_{i,ped}$. This has potentially important consequences for wall impurity evolution on ITER [3,27]. The low values of T_e measured by the TTP during the ELM in the far SOL (Fig. 4) are thus also expected on the basis of the transient model.

The model has also been used to compare with IR measured far SOL average power widths, $\lambda_{W,ELM}$, during wall-outer gap scan experiments, finding $\lambda_{W,ELM}$ ~ 35 mm in very favourable agreement

with measured values of $\lambda_{W,ELM} \sim 33$-35 mm for discharges in which $W_{ELM}/W \sim 0.05$ and $W_{ELM}/W_{ped} \sim 0.12$, with W and W_{ped} respectively the total plasma and pedestal stored energies [27]. This encouraging match between model and experiment may be used as a reference point to construct a more general expression for the ELM filament folding length in the case of varying W_{ELM}/W if a scaling of filament radial velocity with ELM amplitude can be assumed (since the transient model requires that v_r be specified) [27]. If, as suggested very recently, ELM filaments are driven cross-field by interchange motions [25], then larger amplitude events should propagate more rapidly, such that $\lambda_{W,ELM} \approx v_r\tau_{\|} \approx v_r L_{\|}/c_s \rightarrow \lambda_{W,ELM}/L_{\|} \approx v_r/c_s \propto (W_{ELM}/W)^{1/2}$. Combining this scaling with the moderate ELM e-folding length ($\lambda_{W,ELM} \sim 35$ mm for $W_{ELM}/W_{ped} \sim 0.12$) and assuming the mid-pedestal approximation for the start of ELM parallel losses gives a rough estimate for the scaling, in JET, of the expected ELM energy to the main chamber, $W_{ELM,wall}$, as a function of W_{ELM}: $W_{ELM,wall} \approx W_{ELM}\exp(-(\Delta_{ped}/2 + \Delta_{SOL})/\lambda_{W,ELM})$, with $\lambda_{W,ELM} \approx 35(W_{ELM}/0.12W_{ped})^{1/2}$ and where Δ_{ped} is the estimated pedestal width [27].

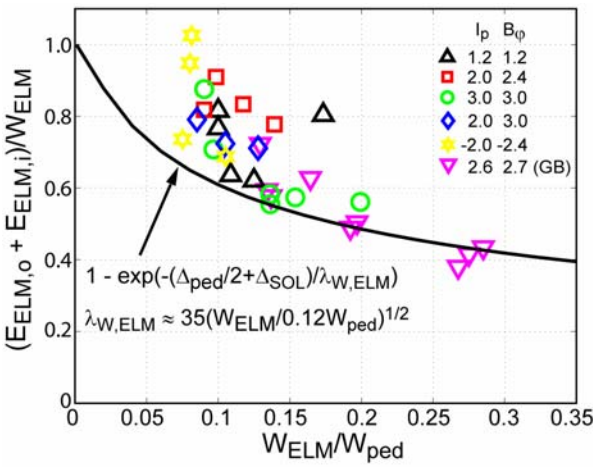

Fig. 6: *Divertor ELM energy fraction vs. normalized ELM energy for DOC-L discharges compared with transient model prediction based on interchange driven ELM amplitude scaling. I_p and B_φ in MA and T respectively. GB=data from discharges in MarkIIGB divertor configuration.*

Although the new wide angle IR should ultimately be able to provide direct estimates of $W_{ELM,wall}$ for a range of W_{ELM}, this is not yet possible. Instead, the model quantity $(1\text{-}W_{ELM,wall}/W_{ELM})$ can be compared with the divertor target ELM energy measurements in Fig. 1, assuming the energy radiated during the ELM to be $<< W_{ELM}$. Figure 6 presents the result of this exercise for the data in Fig. 1 [8], where although ELM energy deposition on divertor tiles 1 (see inset in Fig. 1 for tile numbering) is not visible to the divertor viewing IR camera, an attempt has been made to include it using tile thermocouples to measure the total accumulated energy during the discharge and assuming the ELM energy fraction deposited on Tile 1 is similar to that on Tiles 3,7 and 8 which are in the field of view of the IR measurement. For these DOC-L discharges, $\Delta_{SOL} \sim 4.5$ cm and a representative value of $\Delta_{ped} \sim 3.0$ cm has been assumed. Also included in Fig. 6 are a number of additional points from earlier measurements in the MarkIIGB divertor, for which the same Δ_{SOL}, Δ_{ped} have been applied. Given the approximate nature of the model, and the incomplete total energy balance, agreement with experiment is again fair. As reported previously on the basis of a subset of the data in Fig. 6 [28], the trend for larger ELM events to convect higher fractions of the pedestal energy to the wall is manifest in the experimental data. Extrapolation of this approach to moderate Type I ELMs ($W_{ELM}/W \sim 5\%$) in the ITER reference scenario, predicts that ~8% of W_{ELM} would be deposited on the first limiting flux surface in the upper dump plate region [27].

4. Conclusions

Improving the characterisation and understanding of ELM transport in the SOL and the consequences for first wall and divertor power loading is an important feature of research at JET. Careful analysis of infra-red thermographic measurements of divertor target ELM energy deposition from a series of discharges with varying pedestal ELM energy losses up to $W_{ELM} = 1$ MJ has shown clear evidence for a strong asymmetry favouring the inner target. Except at the lower ELM energies ($W_{ELM} < 100$ kJ), where the data are more scattered, this asymmetry closely follows $E_{ELM,i}/E_{ELM,o} = 2$ and thus counteracts, to some extent, the inter-ELM target energy asymmetry which is heavily weighted towards the outer target, particularly at high input power. An explanation for this ELM energy asymmetry has not yet been found, though JET data show that it is not a function of pedestal collisionality and observations on ASDEX Upgrade demonstrate a clear correlation with divertor target current flows.

PIC simulations of parallel ELM transport under JET like conditions have been considerably improved over earlier efforts, notably with reduced shortening parameters and increased grid resolution. Code runs for a range of W_{ELM} clearly demonstrate how divertor target sheath heat transmission factors vary rapidly during the ELM event, particularly in the case of electrons, for which classically expected values can be exceeded by up to 2 orders of magnitude. Nevertheless, because only about 30% of the ELM energy is carried by the electrons, only at the highest W_{ELM} are the peak target power flux densities significantly overestimated if, as is common practice in edge fluid code simulations, γ is assumed constant through the ELM.

A picture of the ELM as a series of toroidally rotating, field aligned filaments is supported by probe measurements of plasma flux, T_e and hot ion flux in the far SOL. Further evidence is provided by a new wide angle IR camera system which has observed helical stripes of power deposition during ELMs on main chamber and upper dump plate surfaces. Whilst T_e in the ELM filament reaching the wall remains low, ions arrive there with energies characteristic of the pedestal region. This is expected on the basis of a new transient model of ELM filament energy loss which matches this experimental far SOL probe data as well as measured values of ELM SOL e-folding lengths for prescribed radial propagation velocities. If the latter scale with ELM amplitude as predicted on the basis of an event driven by interchange motions, the model also reproduces the observed trend seen in JET for larger ELMs to deposit less energy in the divertor.

Acknowledgement

This work was conducted under European Fusion Development Agreement and was partly funded by EURATOM and the Swiss National Science Foundation.

References

[1] LOARTE A. et al., Phys. Plasmas **11** (2004) 2668
[2] ZHITLUKHIN A. et al., to be published in J. Nucl. Mater.
[3] PITTS R. A. et al., Plasma Phys. Control. Fusion **47** (2005) B303
[4] PITTS R. A. et al., J. Nucl. Mater. **337-339** (2005) 146; [5] FUNDAMENSKI W. et al., ibid. p305
[6] COAD J. P. et al., Nucl. Fusion **46** (2006) 350
[7] ANDREW P. et al., J. Nucl. Mater. **337-339** (2005) 99
[8] EICH T. et al., submitted to Plasma Phys. Control. Fusion
[9] EICH T. et al., to be published in J. Nucl. Mater.
[10] FUNDAMENSKI W., PITTS R. A., Plasma Phys. Control. Fusion **48** (2006) 109
[11] HUBER A., presented at 24th Symposium on Fusion Technology, Warsaw, Poland, 2006
[12] FUCHS J. C. et al., J. Nucl. Mater. **337-339** (2005) 756
[13] BERGMANN A., Nucl. Fusion **42** (2002) 1162
[14] TSKHAKAYA D. et al., Theory of Fusion Plasmas, Italy (2004) ed J. W. Connor et al.
[15] TAKIZUKA T. et al., Contrib. Plasma Phys. **46** (2006) 698
[16] STANGEBY P. C., "The plasma boundary of magnetic fusion devices", 2000 (IOP Publishing)
[17] KIRK A. et al. Plasma Phys. Control Fusion **47** (2005) 315
[18] EICH T. et al., Phys. Rev. Lett. **91** (2005) 195003
[19] GHENDRIH P. et al., J. Nucl. Mater. **313-316** (2003) 914
[20] GAUTHIER E. et al., to be published in J. Nucl. Mater.
[21] ANDREW P. et al., in preparation
[22] HERRMANN A. et al. Plasma Phys. Control Fusion **46** (2004) 971
[23] PITTS R. A. et al., Nucl. Fusion **46** (2006) 82
[24] SILVA C. et al., J. Nucl. Mater. **337-339** (2005) 722
[25] GARCIA O. E. et al., Phys. Plasmas **13** (2006) 082309
[26] FUNDAMENSKI W., SAILER W., Plasma Phys. Control. Fusion **46** (2004) 233
[27] FUNDAMENSKI W., PITTS R. A., to be published in J. Nucl. Mater.
[28] EICH T. et al., J. Nucl. Mater. **337-339** (2005) 669